



Experimental and Analytical Study of High-Strength Concrete Containing Natural Zeolite and Additives

Iswarya Gowram^{1*}, Beulah. M¹

¹ Department of Civil Engineering, School of Engineering and Technology, Christ (Deemed to Be University), Bangalore, 560074, India.

Received 13 July 2022; Revised 19 September 2022; Accepted 26 September 2022; Published 01 October 2022

Abstract

The study compares the durability of Natural Zeolite with Metakaolin, Silica Fume, and Fly Ash on high-strength concrete. 300 concrete specimens were tested for compressive strength before and after an acid attack, modulus of elasticity, water absorption, and rapid chloride permeability. 5%, 10%, and 15% of the cement were replaced with cementitious elements while maintaining the same quantity of Natural Zeolite. In this investigation, the water-cement ratio was maintained at 0.35. After 28 days, the specimens were tested for durability. Samples of all mixes were TG/DT and FTIR tested. The optimal percentages of cementitious materials that resulted to the maximum durability enhancements were reported as the study results. Experimental results showed that Natural Zeolite and Metakaolin strengthened the durability of concrete. All the data show that 5% Natural Zeolite with 10% Metakaolin performs well. Good R^2 values and appropriate independent variable coefficients suggested that the regression findings for high-strength concrete durability were accurate. The P values of all models were less than 0.005 and the F values were statistically significant and appropriate; therefore, the generated models predict concrete's strength with authenticity.

Keywords: Natural Zeolite (NZ); Metakaolin (MK); Silica Fume (SF); Fly Ash (FA); Durability; Regression Analysis.

1. Introduction

Concrete is a popular material choice because of its durability and comparatively low cost. Rapid chloride permeability, water absorption, and acid attack protection are priority properties desired in concrete. A new type of concrete, namely High-Performance Concrete (HPC) has emerged in the construction industry recently with all these desirable qualities and also, as a fallout of advancements in concrete technology. Among high-performance concretes with increased tensile and compressive strength and durability, High-Strength Concrete (HSC), Fiber-Reinforced Concrete (FRC), and Self-Consolidating Concrete (SCC) are the most popular ones. For their wide range of construction applications, these new forms of concrete are often tested for durability [1]. Rapid chloride permeability, drying shrinkage, alkali-aggregate reaction, sulfate resistance, X-ray diffraction test, and SEM are also highly relevant parameters for the durability assessment of construction material properties [2]. Synthetic zeolite from aluminum fluoride by low-temperature synthesis was used as an additional cementitious ingredient to improve the durability of concrete [3].

Experiments showed that including tuff and Natural Zeolite (NZ) significantly increased specimen chloride resistance. The best results in water absorption and chloride diffusion tests were achieved when cement and sand were partially replaced with 10% NZ and 15% tuff, respectively [4]. Self-compacting concrete with 15% NZ was found to be more resistant to acid attacks than conventional concrete. Using pumice as a substitute for 10% of Portland cement

* Corresponding author: gowram.iswarya@res.christuniversity.in

 <http://dx.doi.org/10.28991/CEJ-2022-08-10-019>



© 2022 by the authors. Licensee C.E.J, Tehran, Iran. This article is an open access article distributed under the terms and conditions of the Creative Commons Attribution (CC-BY) license (<http://creativecommons.org/licenses/by/4.0/>).

content increased the concrete's resistance to carbonation by 1.6 times compared to the resistance offered by the control concrete. Additional research on the formulation and characteristics of new concrete incorporating NZ to improve mechanical strength was recommended to improve performance and profits from this natural pozzolan [5]. When a suitable quantity of NZ was added to the paste, the total porosity and pore size of the paste decreased in comparison to the addition of the same quantity of Fly Ash (FA) [6]. A Study revealed that NZ caused the decline of water absorption and chloride permeability. It also increased compressive strength, chloride durability, and electrical resistivity as compared to the same properties of the control concrete [7].

Use of novel cementitious materials for research increased over the last several years [8]. In durability tests, Metakaolin (MK) concrete showed higher resistance than the control concrete, and this resistance improved with increasing MK percentage [9]. A MK based geopolymer concrete was tested for freeze-thaw durability. A blend with a molar ratio of 1.0 produced better durability than a mix with a molar ratio of 1.4 [10]. Using a lower W/B ratio or a greater binder content of MK mixes increased efficacy and decreased the probability of corrosion occurrence [11]. The findings of a study revealed that 10% NZ and 10 % MK combined with micro-nano bubbles of water reduced 24-hr water absorption and chloride penetration by 17.56% and 80.45%, respectively, at 90 days of age, compared to the same properties of the control sample [12]. Using capillary porosity, the chloride penetrability of MK-based concrete was studied to examine the capability of absorption of the chemical [13]. MK from a waste by product was used in concrete as 5 to 15% replacement for cement, and the concrete's durability was evaluated by a chloride penetration test, freeze-thaw test, and alkali-silica reactivity tests [14].

As the Silica Fume (SF) and MK binder contents increase, the resistance of concrete to chloride ion penetration decreases significantly [15]. Mechanical and durability properties of concrete improved significantly by adding SF [16]. In addition to flexural, splitting tensile, and compressive strength tests, the specimens were scanned electron microscopically for chloride penetration and carbonation. The findings showed that specimens made with coarser aggregates and SF performed better than those made with smoother aggregates [17]. The durability of FA and aggregate-based structural lightweight concrete was studied for their water permeability, absorption, and freeze-thaw resistance to determine their long-term applicability in the construction industry [18]. Capillary penetration and water absorption were significantly decreased by the addition of Calcium Stearate (CS). After 120 days of wet curing, the integration of 7 kg/m³ of CS in concrete, decreased the electrical resistivity, total water absorption, and chloride diffusivity by 60%, 72%, and 40%, respectively, compared to the reference mixture without CS and additives [19].

Due to an increasing need for high-performance concretes with high strength and long-term durability, recent structural diversification has increased interest in the material's workability and durability. The addition of nano-silica and SF improved concrete's mechanical properties and durability [20]. The pozzolanic reaction with portlandite enhanced the durability of concrete [21]. When Portland cement is replaced with large proportions of FA and SF, the chloride resistance of SCC can be significantly improved [22].

An acid attack is one of the most severe environmental deteriorations that affect the longevity of concrete structures [23]. Supplementary Cementitious Materials (SCM) increased the acid resistance in concrete, and the addition of natural pozzolan to concrete improved its resistance to sulfuric acid attack. Also, weight loss measurement was shown to be a valid test for concrete resistance to sulfuric acid attack [24]. To test Alkali-Activated Slag (AAS) concrete's acid resistance, it was submerged in a PH 4 acetic acid solution. Compressive strength evolution, degradation products, and microstructural changes were significant characteristics. Grade 40 AAS concrete produced better acid resistance than Grade 40 OPC concrete made using the similar compositions [25].

The determination of the compressive strength of high-strength concrete by experimental techniques was a costly and time-consuming operation, and slight errors resulted in the labour being repeated. Hence, different approaches were utilized to address these drawbacks [26]. Taguchi L16 orthogonal array experimental design optimized concrete's mechanical characteristics. Multiple regression analysis determined fly ash's impact on concrete's mechanical properties [27]. The impact of bottom ash and granite powder on concrete performance was assessed. On the basis of the outcomes of the experiment, regression models were created. The performance of bottom ash concrete improved when granite powder was added [28]. The impact of natural zeolite on the concrete's strength qualities by multiple regression analysis using SPSS tool to provide formulas for strength prediction was performed. The test findings on concrete that has been combined with zeolite in a laboratory were used to verify the predicted results [29].

Therefore, it is evident from the literature that the usage of NZ and additives has a significant effect on the durability properties of the concrete and is an area of research needing further exploration. Therefore, a study has been undertaken to examine the characteristics and performance of the additives and their influence on the durability properties of concrete. The durability assessment of concrete has been carried out by acid attack tests, the Rapid Chloride Permeability Test (RCPT), and water absorption tests.

1.1. Research Significance

Determining the durability properties of HSC with three types of additives was central to this study. This study involved HSC prepared using natural zeolite and an examination of the effects of three dissimilar additives with

varying properties and proportions on HSC durability properties. Regression models developed using SPSS software for the concrete properties were based on the experimental results. The strength reduction due to the acid attack has been computed too.

2. Materials and Methods

2.1. Materials

M sand with a specific gravity of 2.60, was employed as the fine aggregate. The coarse aggregate used in this study had a maximum size of 20 mm, water absorption of 0.4%, and specific gravity of 2.68. Type I ordinary Portland cement (OPC) that conformed to ASTM C 150 [30] and had a 28-day compressive strength of 53 MPa was used to make the concrete sample. NZ, MK, FA, and SF were used as additives for the high strength concrete. The chemical compositions of OPC, NZ, MK, FA, and SF are listed in Table 1. NZ in a constant quantity, MK, FA, and SF in varying proportions were used to prepare the different mixes.

Table 1. Chemical compositions of materials

Chemical properties	Chemical composition (%)												
	Material	SiO ₂	Al ₂ O ₃	Fe ₂ O ₃	TiO ₂	CaO	MgO	Na ₂ O	K ₂ O	LOI	C ₃ S	C ₂ S	C ₃ A
Metakaolin	52.0	46.0	0.60	0.65	0.09	0.03	0.10	0.03	1.00	56.47	20.66	6.31	8.29
Natural NZ	74.3	10.52	1.6	-	4.25	0.6	-	-	5.3	-	-	-	-
SF	99.886	0.043	0.04	0.001	0.001	0	0.003	0.001	0.015	-	-	-	-
Cement	21.25	4.33	1.85	0.13	64.3	1.81	0.17	0.71	1.5	-	-	-	-
Fly Ash	51.1	33.73	3.84	1.5	3.78	4.14	0.46	1.18	0.22	-	-	-	-

Rajasthan, India was the source for both zeolite and kaolin. Pure NZ was separated from the muck at Astrra Chemicals at Chennai, India. The main components of NZ are aluminum, silicon, and oxygen. Astrra Chemicals used kilns to burn kaolin at temperatures of 600 to 850 degrees Celsius to produce MK. FA is produced as a by-product of coal combustion in thermal power facilities near Bangalore.

Cement, NZ, MK, FA, and SF have specific gravity values of 3.15, 2.1, 2.6, 2.7, and 2.63, respectively. To prepare the concrete, a high-range water-reducing admixture (HRWRA), commercially available as modified polycarboxylate ether with a minimum PH value of 6 and a volumetric mass at 20°C of 1.09 kg/litre, was utilized.

The mix design information for mixes calculated in accordance with IS 10262-2019 [31] and is shown in Table 2. Raw materials were weighed in a computerized balance and batched in accordance with the suitable mix percentage. Cement, natural zeolite, fine aggregate, coarse aggregate, Mk, FA, and SF were among the raw components that were measured and properly blended. The mixture was then further supplemented with a superplasticizer solution mixed in water until it was homogenous. Concrete bleeding and segregation were avoided. A pan mixer was used for the concrete mix preparation.

Table 2. Concrete Mix design from IS 10262-2019

Mix	Material	Cement	Natural Zeolite	Metakaolin	Fly Ash	Silica Fume	Fine aggregate	Coarse aggregate	Water-to-cementitious materials ratio (w/cm)	Water	Super plasticizer
M1	5%Z	415	21.85	-	-	-	628	1202	0.35	153	3.1
M2	5%M	393.3	21.85	21.85	-	-	628	1202	0.35	153	3.1
M3	10%M	372	21.85	43.7	-	-	628	1202	0.35	153	3.1
M4	15%M	350	21.85	65.55	-	-	628	1202	0.35	153	3.1
M5	5%FA	393.3	21.85	-	21.85	-	628	1202	0.35	153	3.1
M6	10%FA	372	21.85	-	43.7	-	628	1202	0.35	153	3.1
M7	15%FA	350	21.85	-	65.55	-	628	1202	0.35	153	3.1
M8	5%SF	393.3	21.85	-	-	21.85	628	1202	0.35	153	3.1
M9	10%SF	372	21.85	-	-	43.7	628	1202	0.35	153	3.1
M10	15%SF	350	21.85	-	-	65.55	628	1202	0.35	153	3.1

Note: M1 is a Reference Mix

2.2. Experimental Methods

The experimental and regression analysis involved in the study has been depicted as a flow chart in Figure 1.

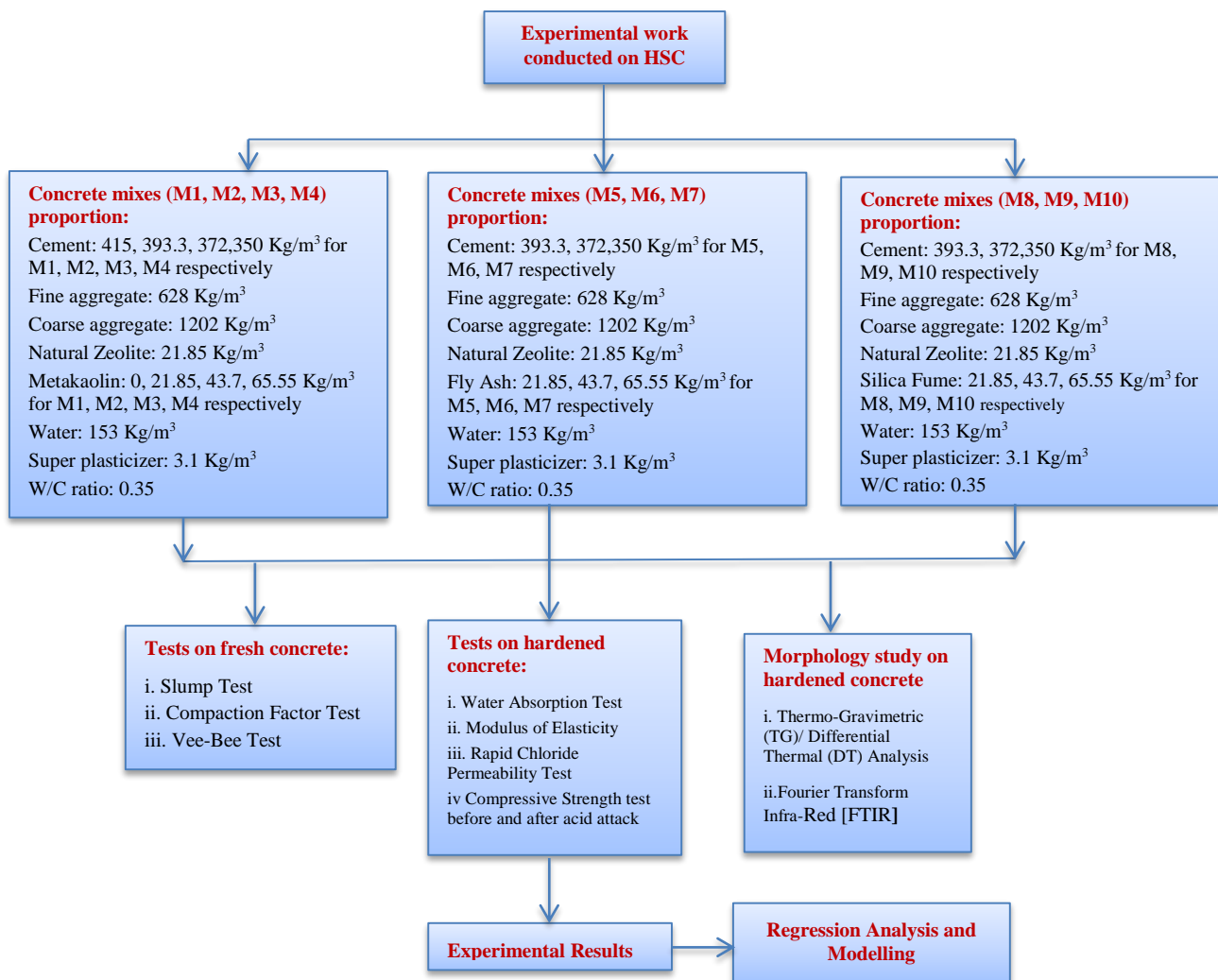


Figure 1. Flowchart of the methodology

2.2.1. Tests on Fresh Concrete

The concrete slump test is used to measure new concrete's consistency before it is set. The workability and flow ability of newly poured concrete is tested using slump cone equipment. It might also be an indication of improper batch mixing. The compaction factor test is a laboratory test for concrete workability. The compaction factor is the weight ratio between partially and compressed concrete. It was developed by the Road Research Laboratory in the UK and is used to judge how well concrete will operate. The compacting factor, or degree of compaction, is calculated using the density ratio, which is the ratio of the density obtained during the test to the density of the same concrete when completely compacted. The compactability and mobility of fresh concrete are demonstrated by the Vee-Bee test.

2.2.2. Tests on Hardened Concrete

After 28 days of curing, the cubes of concrete are submerged in water for 24 hours. The initial weight of the concrete cubes is used to determine the quantity of water they absorb. Calculating and comparing the water absorption of air-dried cubes versus self-cured cubes. The increase in weight relative to the initial weight is represented as its absorption in percentage. The Modulus of Elasticity of concrete is the ratio of applied stress to corresponding strain. It exhibits the stiffness of concrete and its resistance to deformation caused by an applied force. In other terms, it denotes the capacity of concrete to deform elastically. The modulus of elasticity of concrete is a measure of its stiffness, which is a good indicator of its strength. Concrete with a higher modulus of elasticity may withstand more stress before becoming brittle.

To test the capacity of concrete mixes to resist chloride ion penetration, three specimens of each combination were subjected to the test technique after 28 days of curing, outlined in ASTM C1202 [32]. The ASTM C1202 approach

includes measuring the amount of electrical current traveling through a concrete specimen 100 mm in diameter and 50 mm in thickness. When a potential difference of 60 V is maintained across the specimen for six hours, chloride ions are driven to move from a negative-charged NaCl solution through the concrete and into a positive-charged NaOH solution. The steps for preparing concrete disc specimens for testing include one hour of air drying, three hours under a vacuum (80 kPa), one more hour under a vacuum with the specimens submerged in deaerated water, and eighteen hours of soaking in water. The resistance to chloride ion passage is calculated using the total passed charge in coulombs (ASTM C1202-19).

Acid resistance of concrete was assessed in terms of weight loss and residual compressive strength. For this test, 100 mm x 100 mm x 100 mm concrete cubes were cast and kept at 27°C for 24 hours before curing in water for 28 days. After curing for 28 days, the specimens were removed and dried for one day. Initial cube weights were determined. For the acid attack test, 5% of dilute sulphuric acid (H_2SO_4) and Hydrochloric acid (HCl) were added to water with a pH value of around 2. After obtaining initial weights, the cubes were submerged for 60 days in the acidic water described above. After immersion in the aforementioned acidic water, the cubes' weight loss and residual compressive strength are measured. Figure 2 shows the specimens that are ready for the durability tests. Figure 3 shows the experimental setup for RCPT.



Figure 2. Specimens for testing



Figure 3. Experimental Setup for RCPT

3. Results and Discussion

3.1. Fresh Concrete

According to Figure 4, the slump values for fresh concrete mixed with NZ, MK, FA, and SF ranged from 43mm to 58mm. Mix 7 achieved the highest slump value of 58 mm, whereas reference Mix 1 achieved the lowest value of 43 mm. Figure 5 shows that the compaction factor values ranged from 0.81 to 0.9. Mix 7 had a maximum compaction factor value of 0.9; Mix 1 had a minimum value of 0.81. In Figure 6, it was noted that the Vee-Bee test results were between 5 and 10 seconds. Mix 7 achieved the minimum Vee-Bee test time of 5 seconds, while Mix 1 achieved the maximum test time of 10 seconds.

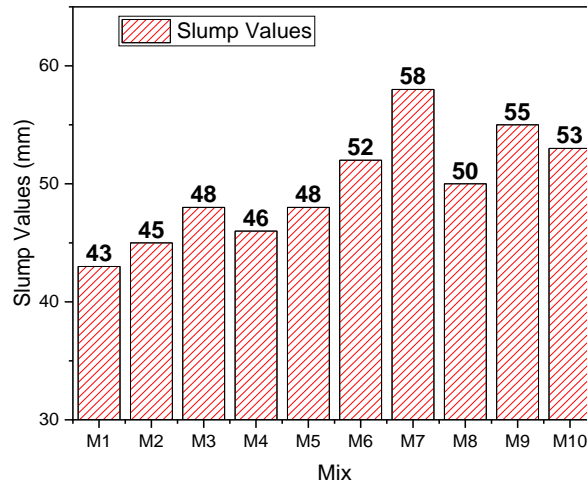


Figure 4. Graph of slump test values for different mixes

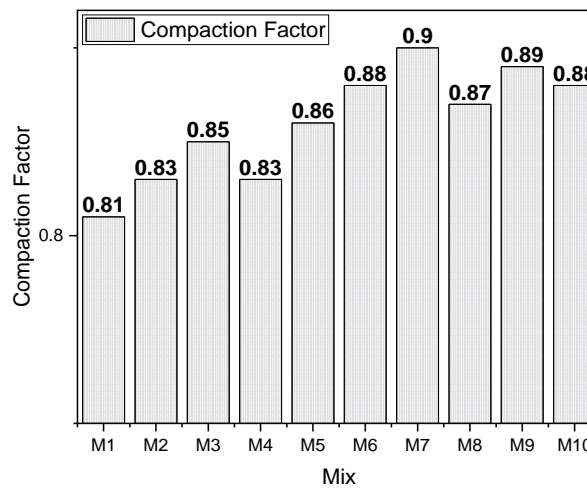


Figure 5. Graph of compaction factor test values for different mixes

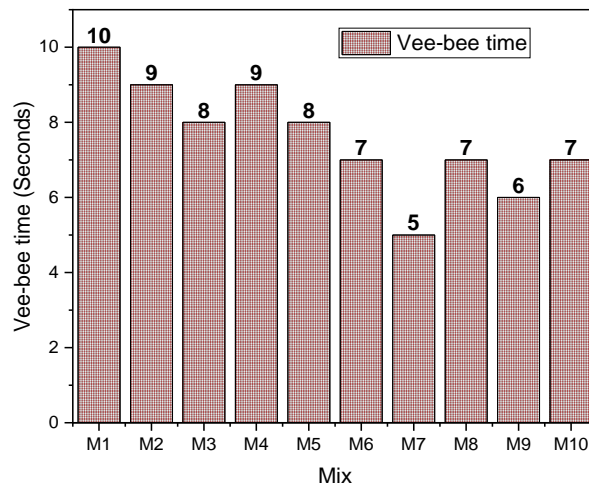


Figure 6. Graph of Vee-Bee test values for different mixes

3.2. Hardened Concrete

According to Figure 7, the water absorption test results for hardened concrete made with NZ, MK, FA, and SF all fell from 1.8% to 2.9%. In terms of water absorption, Mix 3 achieved the lowest percentage (1.8), while Mix 1 achieved the highest percentage (2.9). Figure 8 displays the modulus of elasticity tests. The values range from 35.2 to 43 GPa. Test results showed that Mix 3 had the highest modulus of elasticity at 43 GPa, while Mix 1 had the lowest at 35.2 GPa. The rapid chloride permeability test results for hardened concrete mixed with NZ, MK, FA, and SF ranged from 1018 coulombs to 2162 coulombs, as shown in Figure 9. Reference Mix 1 had reached the maximum value of 2162 coulombs, whereas Mix 3 had the lowest charge passed of 1018 coulombs.

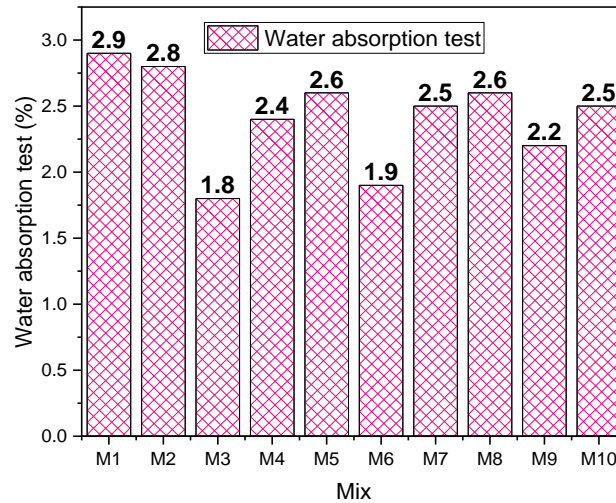


Figure 7. Graph of water absorption test values for different mixes

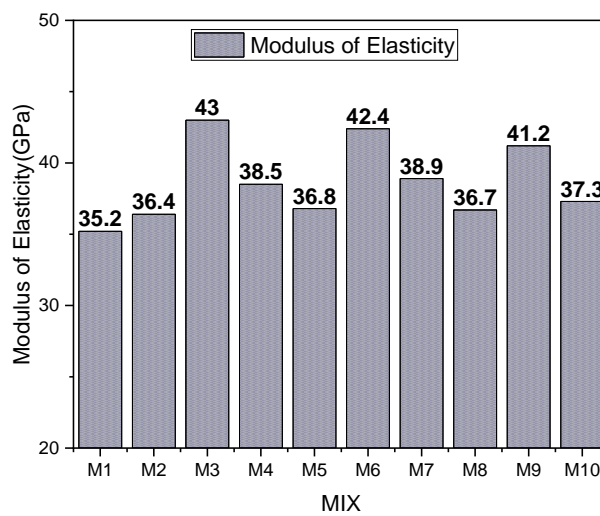


Figure 8. Graph of modulus of elasticity test values for different mixes

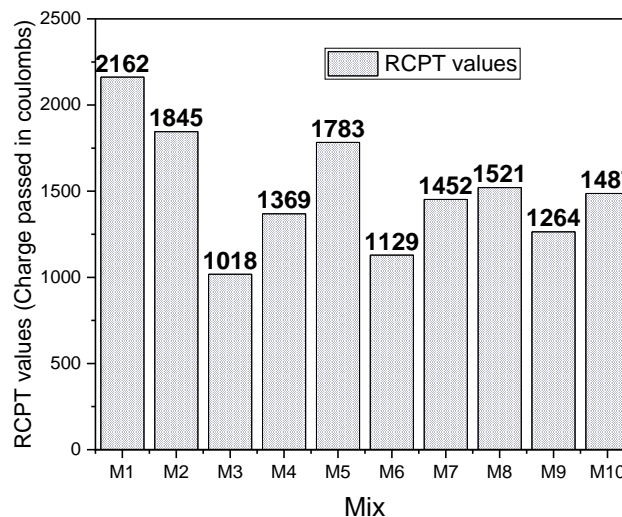


Figure 9. Graph of rapid chloride permeability test values for different mixes

3.3. Compressive Strength Test before and after Acid Attack

According to Figure 10, the compressive strength test results for hardened concrete mixed with NZ, MK, FA, and SF were 63.4 to 48.15 MPa before the acid attack and 61.13 to 42.6 MPa after the acid attack. Compared to the other mixtures, Mix 3 had the highest strength before and after the acid attack.

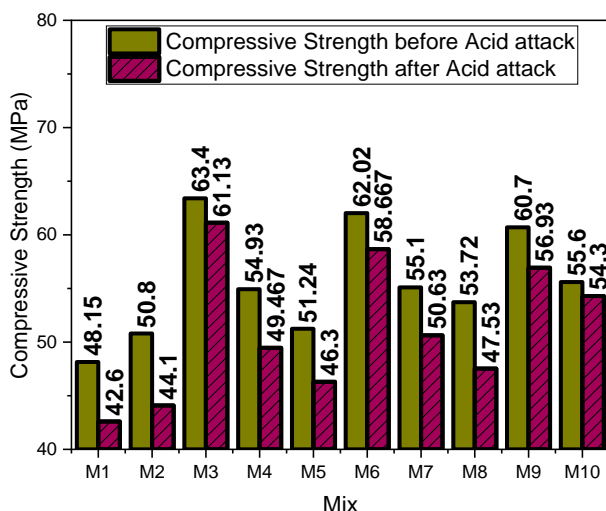


Figure 10. Graph of compressive strength before and after acid attack test values for different mixes

3.4. Strength Loss of Concrete

Figure 11 shows that the values for strength loss for hardened concrete blended with NZ, MK, FA, and SF ranged from 2.34% to 13.19%. The lowest strength loss percentage for Mix 10 was 2.34, while the highest strength loss % for Mix 2 was 13.19.

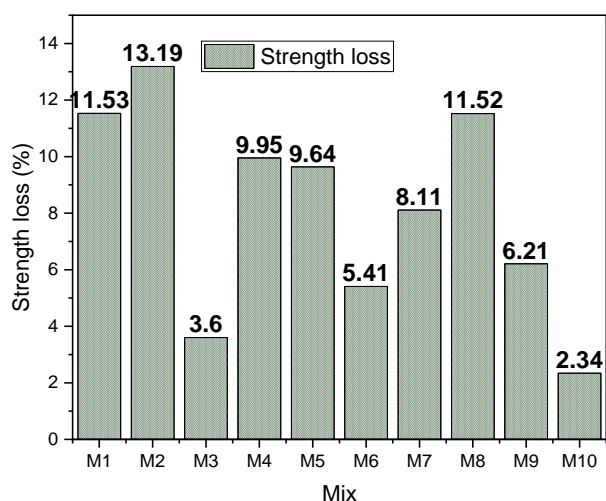


Figure 11. Graph of strength loss for different mixes

The experimental results reflect on the fact that the high strength concrete with Natural Zeolite has exhibited moderate durability properties. When the same design mix with Natural Zeolite and additives such as MK, FA and SF, have shown better durability properties. This enhancement in durability can probably be attributed to additional bonding provided and the reduced porosity due to the presence of a finer material like Silica Fumes.

3.5. Thermo-Gravimetric (TG)/Differential Thermal (DT) Analysis

Using a NETZSCH STA 409PC/PG, samples were subjected to thermo-gravimetric analysis in both standard (heating rate) and high-resolution (10k/min) modes, with temperatures ranging from ambient temperature to 1000° C. Each study utilized a 20mg "nominal" sample. Nitrogen was used for the standard TG/DT analysis. A maximum rate of mass loss (T_{max}) was calculated using the TG/DT analysis of the curves.

Figure 12 displays the results of a TG/DT study conducted on M1, M2, M3, and M4 in a nitrogen atmosphere. When concrete reaches a temperature of 89°C, the water it has absorbed loses its weight. Where there is water absorption, there are also large pores in the mixture that are held to the walls by surface tension. Interlayer water in the concrete's microscopic pores is lost at 132°C. Crystalline structure is altered in size without disintegration when water is lost from interlayers. The weight loss between 423°C and 499°C is due to dehydration of calcium hydroxide, as given by Equation 1, where onset temperature is 429.9°C (peak starts at 441.8°C and ends at 458.1°C) in DT analysis, area under this region is -27.1J/g for M1 mix. The peak between 649°C and 724°C is due to the weight lost by decomposition of $CaCO_3$ and releases of CO_2 , as described in Equation 2.

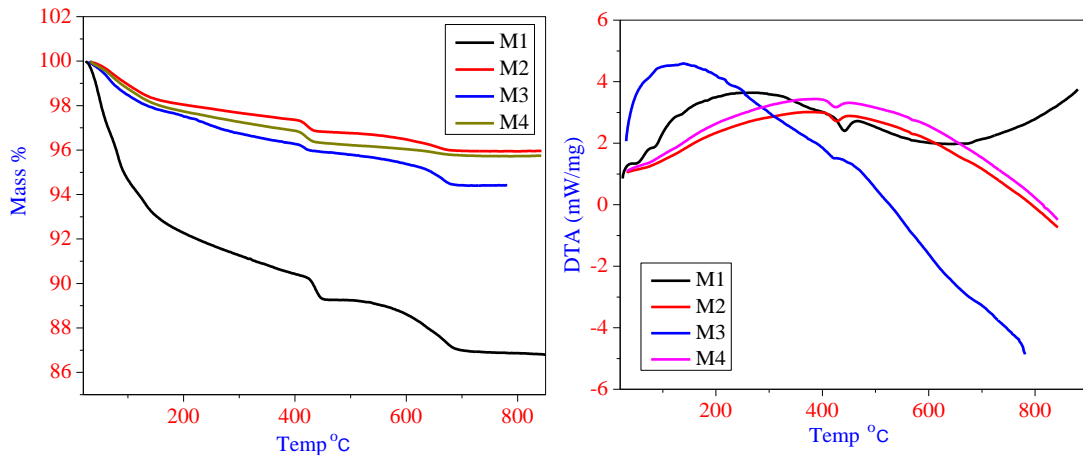


Figure 12. TGA and DTA graphs for M1, M2, M3, and M4 mixes (Metakaolin combination)

For M2, M3, and M4 first degradation peak at 106°C, 98°C, and 113°C, respectively, is attributed to dehydration. Second peaks at 397°C, 402°C, and 400°C are observed. The third peak at 639°C, 645°C, and 647°C is found due to weight loss for M2, M3, and M4, respectively, from TG analysis. From DT analysis for M2, the onset temperature is 411.6°C (peak starts at 426.6°C and ends at 438.9°C), and the area under the peak is -11.76J/g. The onset temperature is 421.3°C (the peak starts at 421.9°C and ends at 428°C), and the area under the peak is -2.149J/g for M3. For M4, DT analysis shows that the onset temperature is 409.1°C (peak starts at 424.6°C and ends at 439.2°C), the area under the peak is -11.67J/g. The exothermic effect (peak Start) followed by endothermic (peak end) for M1, M2, M3, and M4 is mentioned above. The onset thermal deterioration temperature of M1 is 24.602°C; however, after adding MK, thermal stability increases up to 5% MK loading, where the onset thermal degradation temperature is 31°C.

TGA and DTA results of M5, M6, and M7 are shown in Figure 13. It is observed that there is a small amount of weight loss (6% for M5 and M7, and 3% for M6) between 28°C to 133°C, 27°C to 156°C, and 27°C to 149°C for M5, M6, and M7 respectively, attributed to different water content in the concrete mix. The weight loss of around 3% for all the mixes (M5, M6, and M7) is due to the release of free water present in the largest pore of the mixes is between 132°C to 357°C. The peak between 400°C to 440°C refers to the loss of organic material present in the Fly Ash, and it was not reactive during the alkaline activation process. The release above the 500°C can be related to the various carbonate compounds decomposing at a temperature > 850°C. The decomposition of sodium carbonate is reduced between 630°C to 730°C due to the presence of SiO₂.

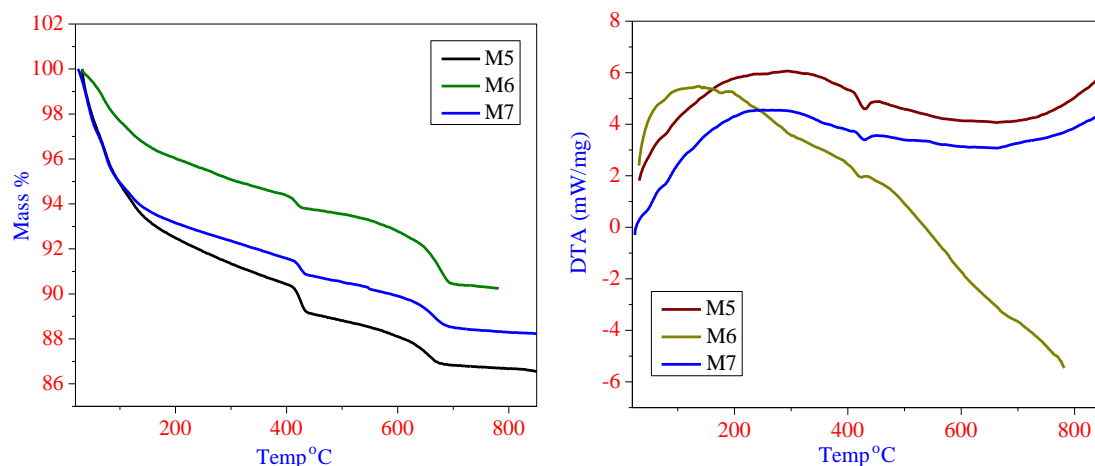


Figure 13. TGA and DTA graphs for M5, M6, and M7 mixes (Fly Ash combination)

Dehydration is responsible for the initial deterioration peak at 143°C, 159.63°C, and 149°C for M5, M6, and M7, respectively. Second maxima are detected at 393°C, 401°C, and 403°C. The third peak is detected at 634°C, 642°C, and 637°C due to weight loss from TG analyses for M5, M6, and M7, respectively. The onset temperature for M5 is 411.8°C (peak starts at 428.5°C and ends at 440.8°C), and the region under the peak is -27.93J/g, according to DT analysis. The onset temperature for M6 is 409.2°C (the peak starts at 420.3°C), and the area under the peak is -8.68J/g.

The onset temperature for M7 is 419.9°C (peak starts at 428.4°C and ends at 440.5°C), and the region under the peak is -14.05J/g, according to DT analysis. The exothermic effect (peak begins) is followed by the endothermic effect (peak ends). The onset thermal deterioration temperature of M5 is 36.673°C; however, after adding Fly Ash, thermal stability is raised to 10% of Fly Ash for mix M6, where the onset thermal degradation temperature is 45.673°C.

Figure 14 displays the M8, M9, and M10 TGA and DTA findings. Dehydration is responsible for M8, M9, and M10 initial deterioration peak, which occurs at 119°C, 102°C, and 117°C, respectively. There are reported second maxima at 399°C, 419°C, and 408°C. Due to weight loss for M8, M9, and M10 via TG analysis, the third peak at 650°C, 656°C, and 660°C is discovered. According to the DT study for M8, the peak temperature is 430°C and ends at 445°C, with a -24.74J/g area under the peak. For M9, the peak area is -8.505J/g, and the onset temperature is 410.3°C (rise starts at 421°C and ends at 431.2°C). According to the DT analysis of M10, the peak temperature is 424°C and ends at 438°C, with a -15.09 J/g area under the peak. The exothermic effect (peak Start) followed by endothermic (peak end) for M8, M9, and M10 is mentioned above.

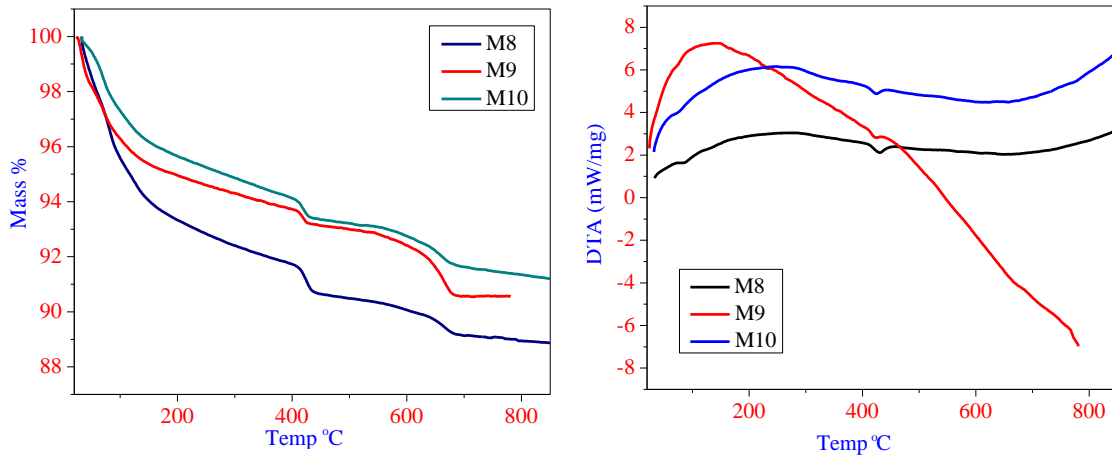


Figure 14. TGA and DTA graphs for M8, M9, and M10 mix (Silica Fume combination)

For M8, the onset temperature of thermal deterioration is 34.166°C; however, adding Silica Fume increases thermal stability up to 15% of Silica Fume in mix M10, where the onset temperature of thermal degradation is 47.074°C.

3.6. Fourier Transform Infra-Red [FTIR]

Figure 15-a refers to FT-IR patterns for Mix1, Mix2, Mix3, and Mix 4. The asymmetric stretching mode of the hydroxyl group of NZ shows in the band around 3750-3200cm⁻¹. At 2940 cm⁻¹ vibrational mode of C-O was observed. At 1422cm⁻¹, it indicates the C-O stretching the carbonate group. The band around 1000-980cm⁻¹ shows aluminum's presence, which confirms the presence of mullite. From Figure 15-b, the symmetric Si-O-Si stretching vibration bond is observed at 774cm⁻¹. The Ca-O bond's vibrations produced another band at 538 cm⁻¹. The vibrations corresponding to the Si-O-Al bond were indexed to a band with an acceptable intensity at 573 cm⁻¹. The results clearly showed the presence of calcium compounds and aluminosilicates in the final system [33].

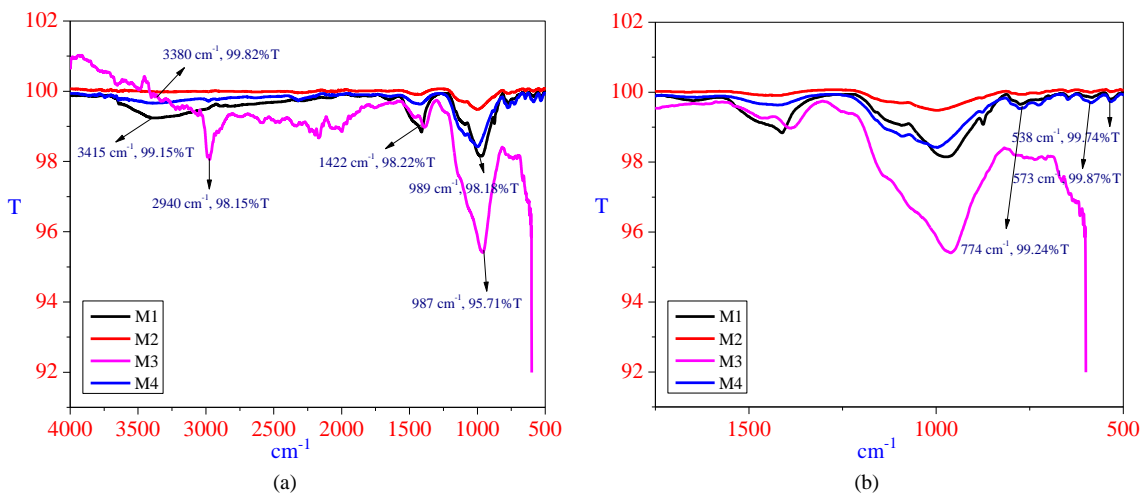


Figure 15. FTIR graph for M1, M2, M3, M4 (Metakaolin mixes)

From Figure 16-a, it is observed that there are six band ranges in the FTIR analysis for Fly Ash mixes. The details of the band area in the range 4000-3400 cm^{-1} show the loss of $\text{Ca}(\text{OH})_2$, the band in between 3400-1400 cm^{-1} indicates elongating of the (-OH) bond and also it shows bending of the (H-O-H) vibrations. From Figure 16-b, the band 1400-1200 cm^{-1} indicates quartz, showing the Si-O-Si bond's gains. 1200-900 cm^{-1} indicate the loss of CaCO_3 and symmetric stretching of the Si-O-Si and Al-O-Si bonds indicated in the 900-500 cm^{-1} band region, and the last band is less than 500 cm^{-1} , indicates the bending vibrations of the Si-O-Si and O-Si-O bonds [34].

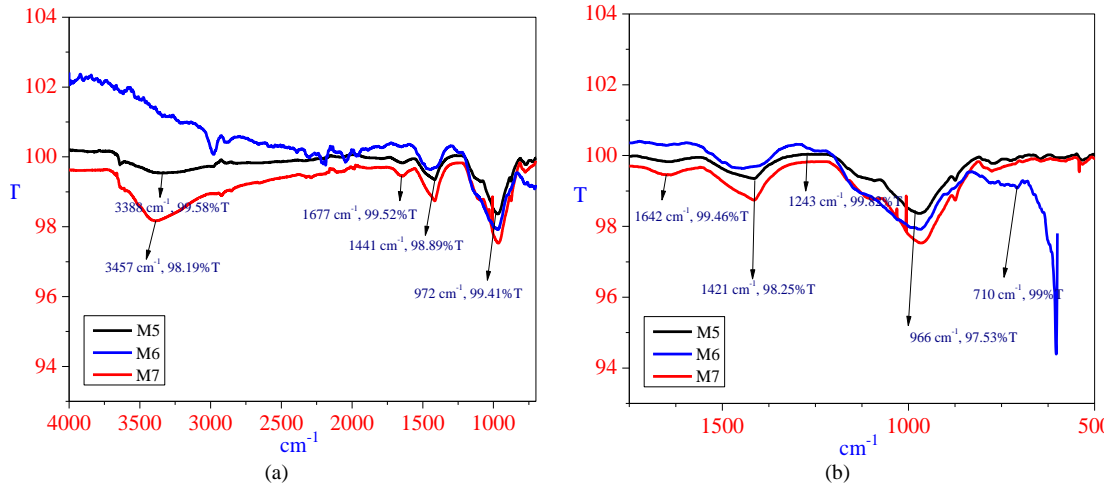


Figure 16. FTIR graph for M5, M6, and M7 (Fly Ash mixes)

FTIR results of Silica Fume in concrete are shown in Figure 17. The band range of 3750-3200 cm^{-1} is due to the stretching vibration of the O-H bond. The absorption band at 2994 cm^{-1} is attributed to the H-O-H stretching, whereas the band at 1439 cm^{-1} is due to the bending vibration of the water molecule. The absorption bands at 983 cm^{-1} and 791 cm^{-1} are attributed to the Si-O-Si bond's asymmetric and symmetric stretching vibration.

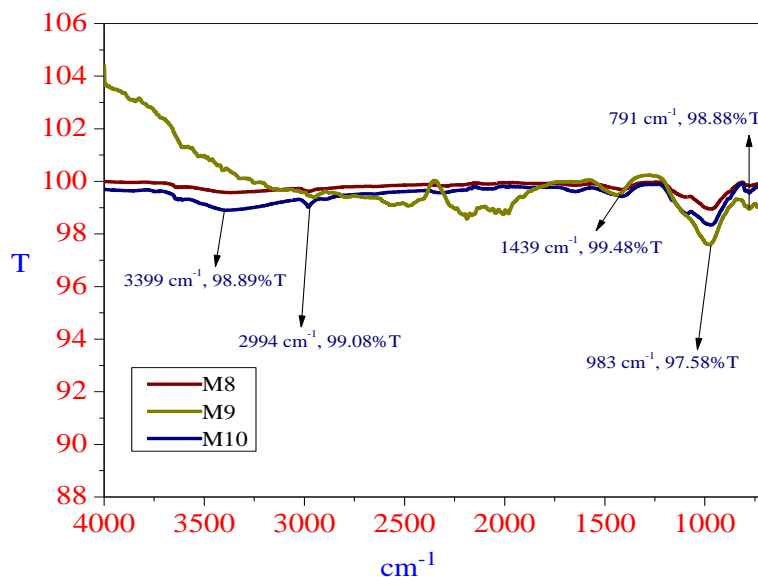


Figure 17. FTIR graph for M8, M9, and M10 (Silica Fume mixes)

FTIR clearly demonstrates the shift in the peaks of tested specimens when the MK, FA and SF additives are present. These peak shifts are not observed in the control mix. These peaks are allegorical of the carbonation extents caused by the additives. The variations observed in the band values for the three additives of MK, FA and SF was due to the hydration of CaCO_3 to varying degrees. Further, a general trend of decrease in these band values have been noticed for increase in concentrations of MK, FA and SF additives barring a few aberrations.

3.7. Regression Analysis

Linear regressions are frequently used statistical methods for approximating a complex relationship between the independent and dependent variables. Linear multivariable regression (LMVR) explains the association between several independent variables and the dependent variable. It entails many strategies for modeling and analyzing certain

variables, mainly when a limited amount of data is available. Stepwise regression identifies the factors that best explain the relationship between the dependent and response variables [35]. It employs an algorithmic strategy to pick the optimal subset of models, which may be achieved by forwarding selection or backward elimination.

The current study developed nine distinct multiple regression models for RCPT, Water absorption, and Acid attack test for NZ, MK, FA, and SF materials with 300 testing sample specimens. Variations were made to the input and output parameters for each regression model. Each model's specifics are detailed in Table 3. The primary purpose of the regression analysis is to predict the durability of concrete for distinct mixtures of composition materials by regressing the RCPT, Water absorption, and Acid attack test against NZ, MK, FA, and SF. The following regression models were tested for the study.

$$RCPT_C = \alpha + \beta_1 * (Z + Meta_M) + \varepsilon_i \quad (3)$$

$$RCPT_C = \alpha + \beta_1 * (Z + Fly_M) + \varepsilon_i \quad (4)$$

$$RCPT_C = \alpha + \beta_1 * (Z + Sil_M) + \varepsilon_i \quad (5)$$

$$WA_{\%} = \alpha + \beta_1 * (Z + Meta_M) + \varepsilon_i \quad (6)$$

$$WA_{\%} = \alpha + \beta_1 * (Z + Fly_M) + \varepsilon_i \quad (7)$$

$$WA_{\%} = \alpha + \beta_1 * (Z + Sil_M) + \varepsilon_i \quad (8)$$

$$AAt_{MPa} = \alpha + \beta_1 * (Z + Meta_M) + \varepsilon_i \quad (9)$$

$$AAt_{MPa} = \alpha + \beta_1 * (Z + Fly_M) + \varepsilon_i \quad (10)$$

$$AAt_{MPa} = \alpha + \beta_1 * (Z + Sil_M) + \varepsilon_i \quad (11)$$

Table 3. Summary of developed models

Model ID	Dependent variable	Independent variable	No. of Samples
Model 1	RCPT (Coulombs)	Metakaolin%	40
Model 2	RCPT (Coulombs)	Fly Ash%	30
Model 3	RCPT (Coulombs)	Silica Fume%	30
Model 4	Water absorption (%)	Metakaolin%	40
Model 5	Water absorption (%)	Fly Ash%	30
Model 6	Water absorption (%)	Silica Fume%	30
Model 7	Acid attack test (MPa)	Metakaolin%	40
Model 8	Acid attack test (MPa)	Fly Ash%	30
Model 9	Acid attack test (MPa)	Silica Fume%	30

Equations 3 to 5 showed multiple regression models for predicting concrete RCPT, whereas Equations 6 to 8 presented multiple regression models for predicting the WA of concrete. Equations 9 to 11 showed the multiple regression models to predict the Acid attack test of concrete, the three dependent variables of RCPT, Water absorption, and Acid attack test; the models were regressed against NZ, MK, FA, and SF.

The final model expressions for the study are as below:

$$RCPT_C = -5.71 (Z + Meta_M) + 99.54 \quad R2 = 81\% \quad (12)$$

$$RCPT_C = -4.43 (Z + Fly_M) + 13.88 \quad R2 = 62\% \quad (13)$$

$$RCPT_C = -3.11 (Z + Sil_M) + 17.85 \quad R2 = 78\% \quad (14)$$

$$WA_{\%} = -3.40 (Z + Meta_M) + 58.10 \quad R2 = 63\% \quad (15)$$

$$WA_{\%} = -0.5 (Z + Fly.M) + 2.86 \quad R2 = 82\% \tag{16}$$

$$WA_{\%} = -0.01 (Z + Sil.M) + 2.43 \quad R2 = 89\% \tag{17}$$

$$AAt_{MPa} = -0.044 (Z + Meta.M) + 2.07 \quad R2 = 72\% \tag{18}$$

$$AAt_{MPa} = -0.01(Z + Fly.M) + 2.53 \quad R2 = 64\% \tag{19}$$

$$AAt_{MPa} = 0.77 (Z + Sil.M) + 43.44 \quad R2 = 69\% \tag{20}$$

For different mix proportions of cement additives, Equations 12 to 14 were developed to predict the RCPT values for MK, FA, and SF respectively. Equations 15 to 17 predicted the water absorption of concrete containing MK, FA, and SF respectively. Acid attack test results can be predicted for HSC containing MK, FA, and SF by Equations 18 to 20 respectively.

On a scale from 0 to 4, the Durbin–Watson statistic was used to determine autocorrelation. As a rule of thumb the value of Durbin-Watson statistics should be in the range between 1.5 and 2.5 [36, 37], to pre-empt autocorrelation issues. Interestingly, each proposed model passed the Durbin-Watson test, indicating that there are no autocorrelation issues in dataset and models’ output. And it is preferable to perform the regression analysis to show the predictability of durability tests.

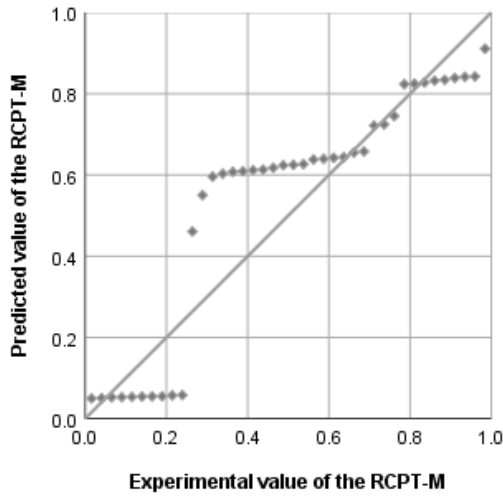
Table 4 illustrates the findings of the multiple regression analysis; models 1-3, respectively, predict the RCPT vs the NZ+MK, NZ+FA, and NZ+SF. It showed that the prediction strength of each model was identical; however, model 1 outperformed models 2 and 3 due to its greater R², F-sig to forecast the RCPT accurately. When water absorption regresses vs. the NZ+MK, NZ+FA, and NZ+SF, respectively, Panel B displays the results of models 4-6. It suggested that model 6, with the combination of NZ and SF, has a higher R2 value and significant F-sig than other combinations; its prediction of water absorption may be more accurate. Models 7-9, which regress NZ+MK, NZ+FA, and NZ+SF, respectively, predict the acid attack test. It indicated that all models performed reasonably similarly, but model 7 performed significantly better than models 8 and 9. It has a perfect Durbin-Watson statistic, an R² of 92%, and a higher F-sig. Overall, this section of the analysis showed that the RCPT, Water absorption, and Acid attack tests we proposed are statistically significant and predictable for durability tests of high-strength concrete.

Table 4. Results of multiple regression analysis (Equations 3 to 11)

S. No.	Model		R ²	p-value	F-sig.	F-value	DW Stat
Panel A: Results from regression model for RCPT							
1	Model 1	NZ + MK	81%	0.000	102.945	0.000	2.07
2	Model 2	NZ + FA	62%	0.000	85.172	0.000	2.46
3	Model 3	NZ + SF	78%	0.000	63.28	0.000	2.48
Panel B: Results from regression model for Water absorption							
4	Model 4	NZ + MK	63%	0.000	74.68	0.000	2.039
5	Model 5	NZ + FA	82%	0.000	71.98	0.000	2.12
6	Model 6	NZ + SF	89%	0.000	129.321	0.000	1.65
Panel C: Results from regression model for Acid attack test							
7	Model 7	NZ + MK	92%	0.000	118.127	0.000	2.004
8	Model 8	NZ + FA	64%	0.000	85.251	0.005	1.60
9	Model 9	NZ + SF	69%	0.000	87.128	0.000	1.54

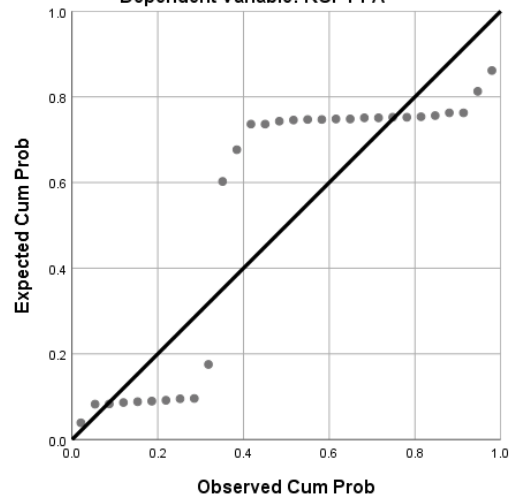
Figures 18-a to 18-c demonstrated a significant correlation between the predicted and experimental values of the dependent variables of the RCPT for each of the three materials (MK, FA, and SF). Table 4 was determined to be consistent with Figures 18-a to 18-i. Figures 18-d to 18-f demonstrated the significant correlation between the predicted and experimental values of Water absorption dependent variables for each of the three materials (MK, FA, and SF). Figures 18-g to 18-i demonstrated a significant correlation between anticipated and experimental acid attack test dependent variable values for each of the three materials (MK, FA, and SF).

Normal P-P Plot of Regression Standardized Residual
Dependent Variable: RCPT M



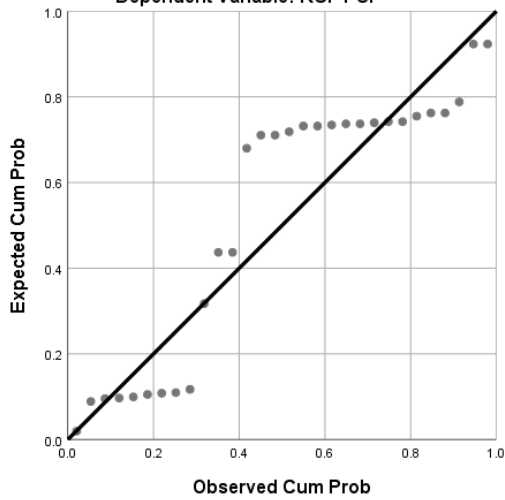
(a) Predicted value Vs. The experimental value of RCPT for Model1

Normal P-P Plot of Regression Standardized Residual
Dependent Variable: RCPT FA



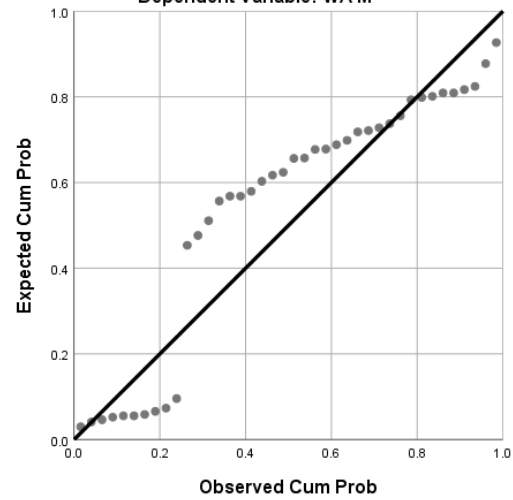
(b) Predicted value Vs. The experimental value of RCPT for Model2

Normal P-P Plot of Regression Standardized Residual
Dependent Variable: RCPT SF



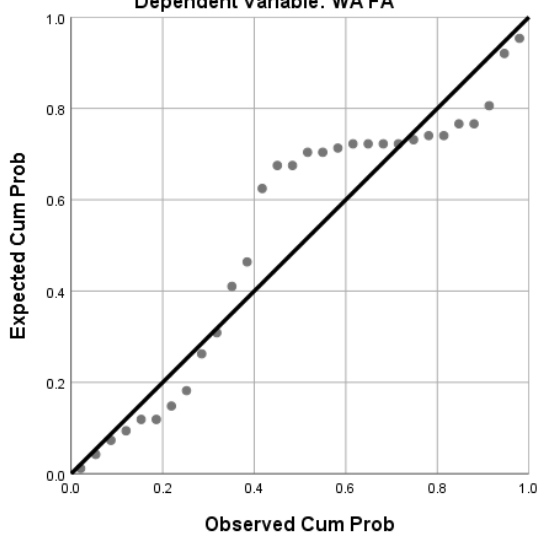
(c) Predicted value Vs. The experimental value of RCPT for Model3

Normal P-P Plot of Regression Standardized Residual
Dependent Variable: WA M



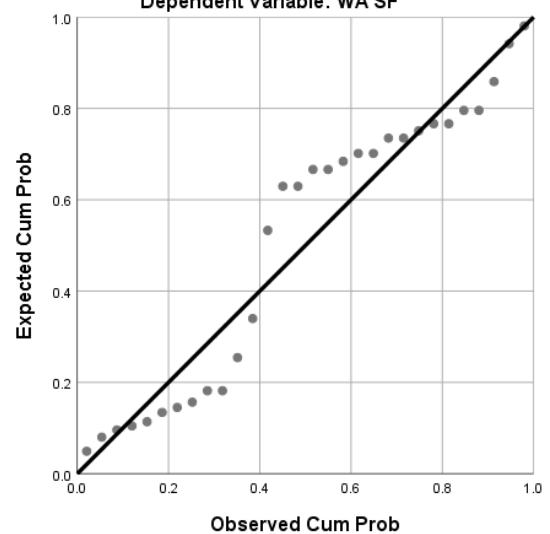
(d) Predicted value Vs. The experimental value of WA for Model4

Normal P-P Plot of Regression Standardized Residual
Dependent Variable: WA FA

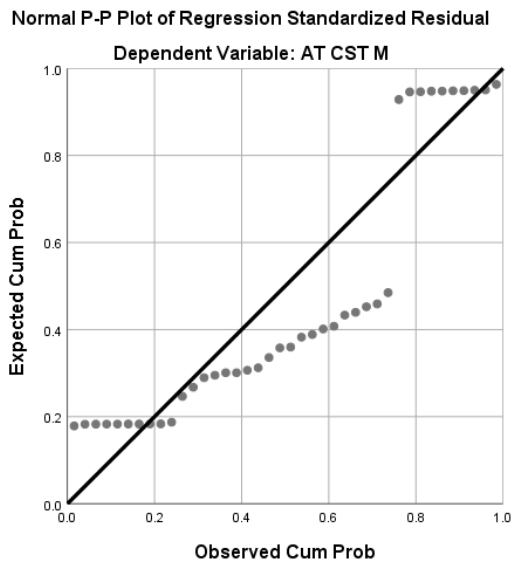


(e) Predicted value Vs. The experimental value of WA for Model5

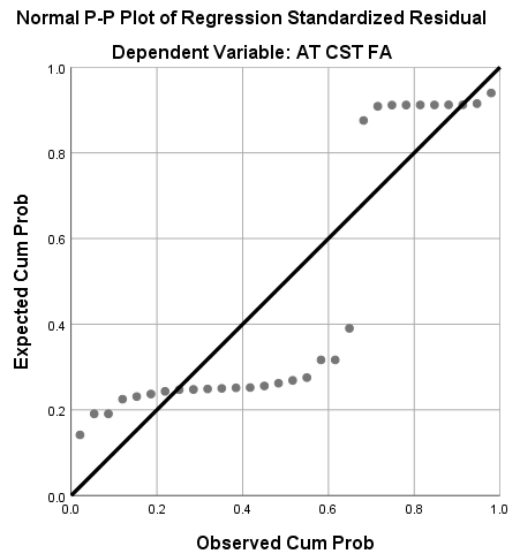
Normal P-P Plot of Regression Standardized Residual
Dependent Variable: WA SF



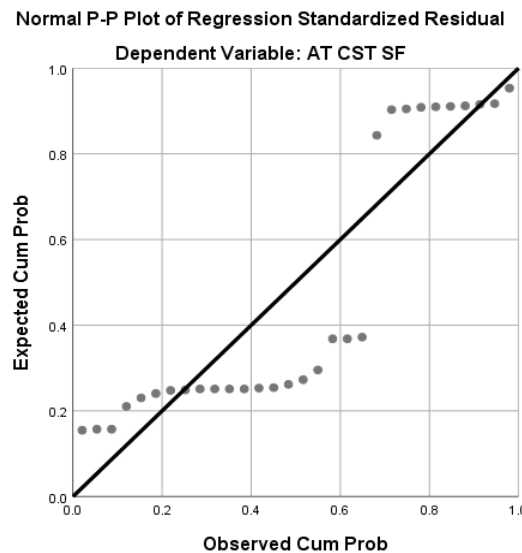
(f) Predicted value Vs. The experimental value of WA for Model6



(g) Predicted value Vs. The experimental value of acid attack CST for Model7



(h) Predicted value Vs. The experimental value of acid attack CST for Model8



(i) Predicted value Vs. The experimental value of acid attack CST for Model 9

Figure 18. Mathematical Regression models for experimental and predicted values of durability parameters

4. Conclusions

In this study, the effects of cementitious materials such as Natural Zeolite along with Metakaolin, Fly Ash, and Silica Fume on high strength concrete were examined experimentally, TG/DT analysis were performed, and statistical models were developed to predict the durability of HSC. The following conclusions emerged from the findings of the experiments and regression models:

- The study proved that the partial replacement of cement by mineral additives, i.e., Natural Zeolite (5% constant) along with Metakaolin, Fly Ash, and Silica Fume, is recommended for better durability and workability.
- The mix (Mix 3) of 10% Metakaolin and a W/C ratio of 0.35 has proven to be the optimal mix with a compressive strength of 63.4 MPa, a modulus of elasticity of 43 GPa, water absorption of 1.8%, and low chloride ion penetration of 1018 coulombs.
- From TG/DT analysis, the thermal stability of a concrete mix containing 10% Metakaolin, 5% Fly Ash, and 15% Silica Fumes was enhanced when compared with other mixes, and the onset thermal deterioration temperatures were 31°C, 45.673°C, and 47.074°C for M3, M5, and M10, respectively, and at these temperatures, the weight loss was due to dehydration of calcium hydroxide.
- FTIR analysis indicated the reduction in CaCO₃ and symmetric stretching of the Si-O-Si and Al-O-Si bonds in different band regions for different additives and their concentrations.

- The regression models have satisfied the Durbin–Watson test without multicollinearity and autocorrelation, and the models can provide a considered statistically reliable prognosis for the durability of high-strength concrete. This is supported by good R^2 values and significant p values for all the models (< 0.005). Also, F-significant values are relatively higher, statistically significant, and adequate.

5. Declarations

5.1. Author Contributions

Conceptualization, G.I.; methodology, G.I.; investigation, G.I.; writing—original draft preparation, G.I.; writing—review and editing, G.I., and B.M. All authors have read and agreed to the published version of the manuscript.

5.2. Data Availability Statement

The data presented in the study are available in the article.

5.3. Funding

The authors received no financial support for the research, authorship, and/or publication of this article.

5.4. Acknowledgements

We would like to thank Dr. Janita Saji, Prof. Sudhir M R and Mr. Bhumiswor Sharma for their expertise and assistance throughout all aspects of our study.

5.5. Conflicts of Interest

The authors declare no conflict of interest.

6. References

- [1] Kodur, V., & Khaliq, W. (2011). Effect of Temperature on Thermal Properties of Different Types of High-Strength Concrete. *Journal of Materials in Civil Engineering*, 23(6), 793–801. doi:10.1061/(asce)mt.1943-5533.0000225.
- [2] Maheshbabu, V., Devi, B. A., & Maheshbabu, B. (2019). Experimental analysis on strength and durability of concrete with partial replacement of Natural Zeolite and Manufactured Sand. *International Journal for Advance Research and Development*, 4(9), 21–26.
- [3] Girskas, G., Skripkiunas, G., Šahmenko, G., & Korjakins, A. (2016). Durability of concrete containing synthetic zeolite from aluminum fluoride production waste as a supplementary cementitious material. *Construction and Building Materials*, 117, 99–106. doi:10.1016/j.conbuildmat.2016.04.155.
- [4] Mohseni, E., Tang, W., & Cui, H. (2017). Chloride diffusion and acid resistance of concrete containing zeolite and tuff as partial replacements of cement and sand. *Materials*, 10(4), 372. doi:10.3390/ma10040372.
- [5] Samimi, K., Kamali-Bernard, S., & Maghsoudi, A. A. (2018). Durability of self-compacting concrete containing pumice and zeolite against acid attack, carbonation and marine environment. *Construction and Building Materials*, 165, 247–263. doi:10.1016/j.conbuildmat.2017.12.235.
- [6] Jitchaiyaphum, K., Sinsiri, T., Jaturapitakkul, C., & Chindapasirt, P. (2013). Cellular lightweight concrete containing high-calcium fly ash and natural zeolite. *International Journal of Minerals, Metallurgy and Materials*, 20(5), 462–471. doi:10.1007/s12613-013-0752-1.
- [7] Ramezaniapour, A. A., Mousavi, R., & Kalhori, M. (2014). Influence of zeolite additive on chloride durability and carbonation of concretes. *Applied mathematics in Engineering, Management and Technology*, 1081–1093.
- [8] Ma, C., Yi, G., Long, G., & Xie, Y. (2019). Properties of High-Early-Strength Aerated Concrete Incorporating Metakaolin. *Journal of Materials in Civil Engineering*, 31(10), 4019225. doi:10.1061/(asce)mt.1943-5533.0002823.
- [9] Dinakar, P., Sahoo, P. K., & Sriram, G. (2013). Effect of Metakaolin Content on the Properties of High Strength Concrete. *International Journal of Concrete Structures and Materials*, 7(3), 215–223. doi:10.1007/s40069-013-0045-0.
- [10] Alanazi, H., Yang, M., Zhang, D., & Gao, Z. (2017). Early strength and durability of metakaolin-based geopolymer concrete. *Magazine of Concrete Research*, 69(1), 46–54. doi:10.1680/jmacr.16.00118.
- [11] Al-alaily, H. S., A. Hassan, A. A., & Hussein, A. A. (2017). Probabilistic and Statistical Modeling of Chloride-Induced Corrosion for Concrete Containing Metakaolin. *Journal of Materials in Civil Engineering*, 29(11), 4017205. doi:10.1061/(asce)mt.1943-5533.0002062.
- [12] Mohsen Zadeh, P., Saghravani, S. F., & Asadollahfardi, G. (2019). Mechanical and durability properties of concrete containing zeolite mixed with meta-kaolin and micro-nano bubbles of water. *Structural Concrete*, 20(2), 786–797. doi:10.1002/suco.201800030.

- [13] Wang, X. Y. (2017). Analysis of hydration-mechanical-durability properties of metakaolin blended concrete. *Applied Sciences* (Switzerland), 7(10). doi:10.3390/app7101087.
- [14] Bumanis, G., Bajare, D., & Korjakins, A. (2016). Durability of High Strength Self Compacting Concrete with Metakaolin Containing Waste. *Key Engineering Materials*, 674, 65–70. doi:10.4028/www.scientific.net/kem.674.65.
- [15] Kim, H. S., Lee, S. H., & Moon, H. Y. (2007). Strength properties and durability aspects of high strength concrete using Korean metakaolin. *Construction and Building Materials*, 21(6), 1229–1237. doi:10.1016/j.conbuildmat.2006.05.007.
- [16] Faraj, R. H., Sherwani, A. F. H., & Daraei, A. (2019). Mechanical, fracture and durability properties of self-compacting high strength concrete containing recycled polypropylene plastic particles. *Journal of Building Engineering*, 25, 100808. doi:10.1016/j.jobbe.2019.100808.
- [17] Kim, S. S., Qudoos, A., Jakhrani, S. H., Lee, J. B., & Kim, H. G. (2019). Influence of coarse aggregates and Silica Fume on the mechanical properties, durability, and microstructure of concrete. *Materials*, 12(20), 3324. doi:10.3390/ma12203324.
- [18] Domagała, L. (2020). Durability of structural lightweight concrete with sintered fly ash aggregate. *Materials*, 13(20), 4565. doi:10.3390/ma13204565.
- [19] Naseroleslami, R., & Nemati Chari, M. (2019). The effects of calcium stearate on mechanical and durability aspects of self-consolidating concretes incorporating silica fume/natural zeolite. *Construction and Building Materials*, 225, 384–400. doi:10.1016/j.conbuildmat.2019.07.144.
- [20] Fallah, S., & Nematzadeh, M. (2017). Mechanical properties and durability of high-strength concrete containing macropolymeric and polypropylene fibers with nano-silica and silica fume. *Construction and Building Materials*, 132, 170–187. doi:10.1016/j.conbuildmat.2016.11.100.
- [21] Karakurt, C., & Topu, L. B. (2012). Effect of blended cements with natural zeolite and industrial by-products on rebar corrosion and high temperature resistance of concrete. *Construction and Building Materials*, 35, 906–911. doi:10.1016/j.conbuildmat.2012.04.045.
- [22] Wongkeo, W., Thongsanitgarn, P., Ngamjarrojana, A., & Chaipanich, A. (2014). Compressive strength and chloride resistance of self-compacting concrete containing high level fly ash and silica fume. *Materials and Design*, 64, 261–269. doi:10.1016/j.matdes.2014.07.042.
- [23] Al-Akhras, N. M. (2006). Durability of metakaolin concrete to sulfate attack. *Cement and Concrete Research*, 36(9), 1727–1734. doi:10.1016/j.cemconres.2006.03.026.
- [24] Hordijk, D. A., & Luković, M. (Eds.). (2017). *High Tech Concrete: Where Technology and Engineering Meet*. Proceedings of the 2017 Fib Symposium, 12-14 June, 2017, Maastricht, the Netherlands, Springer. doi:10.1007/978-3-319-59471-2.
- [25] Bakharev, T., Sanjayan, J. G., & Cheng, Y. B. (2003). Resistance of alkali-activated slag concrete to acid attack. *Cement and Concrete Research*, 33(10), 1607–1611. doi:10.1016/S0008-8846(03)00125-X.
- [26] Mandal, S., Shilpa, M., Rajeshwari, R. (2019). Compressive Strength Prediction of High-Strength Concrete Using Regression and ANN Models. *Sustainable Construction and Building Materials*. Lecture Notes in Civil Engineering, 25, Springer, Singapore. doi:10.1007/978-981-13-3317-0_41.
- [27] Kate, G. K., Nayak, C. B., & Thakare, S. B. (2021). Optimization of sustainable high-strength-high-volume fly ash concrete with and without steel fiber using Taguchi method and multi-regression analysis. *Innovative Infrastructure Solutions*, 6(2), 1–18. doi:10.1007/s41062-021-00472-6.
- [28] Balasubramaniam, T., & Stephen, S. J. (2022). Influence of industrial wastes on the mechanical and durability characteristics of high strength concrete. *Construction and Building Materials*, 317, 126202. doi:10.1016/j.conbuildmat.2021.126202.
- [29] Waghmare, S., Katdare, A., & Patil, N. (2021). Studies on computing compressive strength of zeolite blended concrete using multiple regression analysis. *Materials Today: Proceedings*, 49, 1239–1245. doi:10.1016/j.matpr.2021.06.296.
- [30] ASTM C150-07. (2012). *Standard Specification for Portland Cement*. ASTM International, Pennsylvania, United States. doi:10.1520/C0150-07.
- [31] IS 10262: 2019. (2019). *Concrete Mix Proportioning Guidelines*. Bureau of Indian Standards, New Delhi, India.
- [32] ASTM C1202-19. (2022). *Standard Test Method for Electrical Indication of Concrete's Ability to Resist Chloride Ion Penetration*. ASTM International, Pennsylvania, United States. doi:10.1520/C1202-19.
- [33] Kuzielová, E., Slaný, M., Žemlička, M., Másilko, J., & Palou, M. T. (2021). Phase composition of silica fume—portland cement systems formed under hydrothermal curing evaluated by ftir, xrd, and tga. *Materials*, 14(11), 2786. doi:10.3390/ma14112786.

- [34] Dileep, P., Varghese, G. A., Sivakumar, S., & Narayanankutty, S. K. (2020). An innovative approach to utilize waste silica fume from zirconia industry to prepare high performance natural rubber composites for multi-functional applications. *Polymer Testing*, 81, 106172. doi:10.1016/j.polymertesting.2019.106172.
- [35] Mohd, M. A. B. A., Jamaludin, L., Hussin, K., Binhussain, M., Ghazali, C. M. R., & Izzat, A. M. (2013). Study on Fly Ash Based Geopolymer for Coating Applications. *Advanced Materials Research*, 686, 227–233. doi:10.4028/www.scientific.net/amr.686.227.
- [36] Gowram, I., M, B., Sudhir, M., Mohan, M. K., & Jain, D. (2021). Efficacy of Natural Zeolite and Metakaolin as Partial Alternatives to Cement in Fresh and Hardened High Strength Concrete. *Advances in Materials Science and Engineering*, 2021, 1–10. doi:10.1155/2021/4090389.
- [37] Sharma, B., & Srikanth, P. (2021). Research & development premium in the Indian equity market: An empirical study. *Asian Economic and Financial Review*, 11(10), 816–828. doi:10.18488/JOURNAL.AEFR.2021.1110.816.828.